Granular Matter (2019) 21:32
https://doi.org/10.1007/s10035-019-0886-6

ORIGINAL PAPER

Modeling of granular column collapses with $\mu(I)$ rheology using smoothed particle hydrodynamic method

A. M. Salehizadeh[1] · **A. R. Shafiei**[1]

Received: 4 December 2018 / Published online: 20 March 2019

Abstract
In this paper, to simulate free surface flows of granular materials in a dense regime as a continuum media, a 2D SPH model is developed. The dense flow is characterized as a pressure dependent visco-plastic material based on a local constitutive law to calculate effective viscosity related to local pressure and the norm of strain rate tensor in the numerical method. A simple regularization technique is proposed to reproduce stopping condition and the free surface of a granular flow where the pressure vanishes. Pressure fluctuation as the main drawback of the weakly compressible SPH method leads to an inaccurate pressure distribution. This numerical instability increases at the free surface due to errors associated with the truncated kernels. In this work, a new algorithm is proposed to remove the nonphysical fluctuations by relating divergence of velocity to the Laplacian of pressure. The algorithm is validated for reproducing the dynamics and deposits of collapsing granular columns. The excellent agreement with experimental data is obtained. The maximum thickness of a granular flow on a rough inclined plane is obtained based on the local rheology model. The run-out distances and slopes of the deposits in the simulations also show good agreement with the values found in the experiments.

Keywords Dense granular material · SPH · Pressure dependent visco-plastic material

1 Introduction

The mechanical behavior of the dry granular material flows is of great importance in various fields, including geophysics, physics, and industry. A lot of theoretical and empirical research has been devoted to this topic, especially for determining the mechanical properties of the granular flow.

Based on the velocity and conditions of the granular material flow, the following three regimes are considered: (a) Pseudo-static state or plastic flow for low velocities. (b) The viscous or fluid regime(dense state) in which the particles flow through contact interactions. (c) Gaseous regime when the granular particles have high velocity variations and the main interaction of the particles is a binary collision. Theories described for the flow of granular materials are different in each other. However, due to the frequency of application, the study of the dense state for granular flows is of great interest.

The spreading of collapsing columns of sand and other granular materials on a flat surface has been studied using both experimental and computational methods. Lajeunesse et al. [1, 2] and Lube et al. [3–5] provide an extensively documented set of experimental case studies. These experiments mainly performed on horizontal planes in channels. Also Pouliquen [6] and Mangeney et al. [7] describe laboratory experiments of granular material flowing over an inclined plane covered by an erodible bed.

Many numerical methods have been used to simulate granular flow. One of the most accurate numerical methods to simulate flowing granular media is the Discrete Element Method (DEM) [8]. The first application of DEM to model granular flows was proposed by Cleary et al. [9]. Further improvements have been described in [10–12]. The DEM method solves the classical equations of motion on each grain individually. In spite of its conceptual simplicity, unfortunately, DEM results in untenable computational expense over the large physical domains in geological applications.

✉ A. R. Shafiei
arshafiei@yazd.ac.ir

A. M. Salehizadeh
msalehi@stu.yazd.ac.ir

[1] Mechanical Engineering, Yazd University, Yazd, Iran

One way to describe dry granular flows is to use constitutive equations that express them as a continuum and incompressible media, such that the shear stress is calculated by the particle displacement. The continuum rheology models provided by Da Cruz et al. [13] and Jop et al. [14], as well as the generalized non-local relation by Kamrin et al. [15] for granular flow, have yielded significant improvements compared to the rate-dependent Drucker–Prager [16] model for modeling problems with relatively high strain rates (zones of dense). The volume of fluid (VOF) method has been used in Lagr'ee et al. [17] and the finite-element method (FEM) was used in Kamrin [18]. While both methods provide acceptable results for simple problems, the VOF method has difficulties with extensional disconnection, and cannot determine truly static zones.

On the other hand, Mesh-free particle methods are effective for solving free surface problems. The smoothed particle hydrodynamics (SPH) is a mesh-free Lagrangian method developed by Lucy [19] and Gingold and Monaghan [20] to solve astrophysical problems. It has been successfully applied to a huge range of applications such as the dynamic response of material strength [21, 22], turbulent flow [23] and free surface flows [24–26]. Laigle et al. [27] and Pasculi et al. [28] performed SPH simulation for mudflows using Bingham-type fluids and Bui et al. [29] and Nguyen et al. [30] used elastic–plastic relations to model soil failure flows. Based on empirical studies conducted by Jop et al. [14] and Pouliquen et al. [31], a so-called, $\mu(I)$, local constitutive law was suggested and demonstrated to be effective in describing the dense granular flow. This model correlates the tangential stress to normal stress with dimensionless inertial number I, which characterizes the local state of granular packing.

In a method for the modeling of incompressible flows, an appropriate state equation that correlates pressure changes with density changes is used. This approach is known as the weakly compressible smoothed particle hydrodynamics (WCSPH). In this method, numerical instabilities on the free surface are due to the incompleteness of the kernel support domain and the error in determining the free surface location [32]. In this work, a new algorithm is proposed which can be useful for modeling free-surface flows to produce accurate and stable results. In this algorithm, the divergence of velocity is linked to the Laplacian pressure in the equation of mass conservation. The velocity–pressure coupling, eliminate non-physical oscillations. Also, the gradient of interpolation function is normalized using the correction tensor of first-order derivatives. Although these enhancements have been examined separately, the simultaneous use of these reforms leads to a stable and consistent approach.

The purpose of this work is to use the local rheology model in a proposed SPH algorithm for the simulation of complex free surface dense granular flows. The paper is organized as follows: Sect. 2 describes the governing equations used to simulate free-surface flows of granular materials. The brief introduction to SPH is presented in Sect. 3 then modified SPH algorithm is discussed in Sect. 4. Section 5 reviews the formulation of the constitutive law; The validation of the model is performed in Sect. 6 by reproducing few simple free-surface flow test cases and by reproducing experimental measurements of granular material collapses by Lube et al. [3, 4] and Mangeney et al. [7]. The discussion and conclusions are given in Sects. 7 and 8.

2 The Governing equations

In the present work, the granular material is considered as a fluid that moves with a field flow based on a "continuum" approach. The governing equations for a continuum flow are presented in the following Lagrangian form:

$$\frac{d\rho}{dt} = -\rho \nabla.\mathbf{v} \tag{1}$$

$$\frac{d\mathbf{v}}{dt} = -\frac{\nabla p}{\rho} + \frac{1}{\rho}\nabla.(\mu\nabla\mathbf{v}) + \mathbf{g} + \frac{\nabla.\boldsymbol{\tau}}{\rho} \tag{2}$$

where, ρ and μ are density and dynamic viscosity of the fluid, $\mathbf{v}$ is the velocity vector of the fluid and p is the pressure of the fluid. $\mathbf{g}$ is gravity acceleration, and t indicates time. The sub-particle scale (SPS) stress tensor $\boldsymbol{\tau}$ is necessary to represent the effects of eddy viscosity with a coarse spatial resolution, and its application into the particle simulation has been initially developed by Gotoh et al. [33]. The SPS model has been applied successfully in several free surface problems in SPH [23, 34]. The SPS stress in the particle simulation needs to be modeled for introducing an effect of the eddy viscosity. The SPS stress is represented as [23]:

$$\tau_{ij} = \rho\left(2\nu_t\dot{\varepsilon}_{ij} - \frac{2}{3}k_{sps}\delta_{ij}\right) \tag{3}$$

Where k_{sps} and ν_t are the kinetic energy and the eddy viscosity, respectively. $\dot{\varepsilon}_{ij}$ indicates the strain rate of the flow (i and j here denote spatial coordinates). It is assumed that, the eddy viscosity and the kinetic energy are modeled by the static Smagorinsky model as:

$$\nu_t = \left(c_s\Delta x\right)^2\dot{\gamma} \tag{4}$$

$$k_{sps} = \left(\frac{\nu_t}{0.08\Delta x}\right)^2 \tag{5}$$

where c_s is Smagorinsky constant and is equal to 0.2, Δx is the initial particle spacing and $\dot{\gamma} = \sqrt{2\dot{\varepsilon}_{ij} : \dot{\varepsilon}_{ij}}$ is the norm of strain rate tensor, where, the components of the rate of strain tensor can be written as:

$$\dot{\varepsilon}_{ij} = \frac{1}{2}\left(\frac{\partial v_i}{\partial x_j} + \frac{\partial v_j}{\partial x_i}\right) \tag{6}$$

In SPH method, the dry granular material is assumed to behave as a quasi-compressible material. It is approximated by an artificial material that is more compressible than the real one. The pressure term in Eq. (2) is calculated using an equation of state, which has a function of density change; thus, the pressure equation of granular material will obey Hooke's law [35]:

$$p = K\frac{\Delta V}{V} = K\left(\frac{\rho}{\rho_0} - 1\right) \tag{7}$$

Where K is the bulk modulus, V is the volume, $\Delta V/V$ is the volumetric strain, and ρ_0 is the initial density of the soil. K should be chosen as small as possible in order to ensure a near incompressibility condition. In this study, we chose $K = 50\rho_0 g H_{\max}$ (50 times the maximum initial pressure) [35], where $H_{\max}$ is the initial height of the granular column. This kind of approach for setting up SPH computations is usually referred to as weakly compressible SPH (WCSPH).

3 Smoothed particle hydrodynamics (SPH) formulation

In SPH, The integral representation of function A is approximated by a smoothing kernel function $w_h(|r - r'|)$, with a smoothing length h:

$$A(r) \approx \int_{\Omega} A(r')\, W_h(|r - r'|)\, dr' \tag{8}$$

Where Ω is the supporting domain. The particle approximation of Eq. (10) for particle a, can be written as [36]:

$$A(r_a) \approx \sum_b \forall_b A(r_b)\, W_h(r_{ab}) \tag{9}$$

Where $\forall_b$ is the volume of particle b, r_{ab} is the distance between particles a and b, particle b is in the support domain of particle a. Hereafter $W_h(r_{ab}) = W_h(|r_a - r_b|)$ will be simply written as: W_{ab}.The choice of smoothing kernel function in SPH will directly affect accuracy, efficiency, and the stability of the numerical algorithm. In this study, the cubic B-spline kernel proposed by Monaghan and Lattanzio [37] was used:

$$W_h(r) = \alpha_D \begin{cases} 1 - \frac{3}{2}q^2 + \frac{3}{4}q^3 & 0 \le q \le 1 \\ \frac{1}{4}(2-q)^3 & 1 \le q \le 2 \\ 0 & q \ge 2 \end{cases} \tag{10}$$

where α_D is $\frac{10}{7\pi h^2}$ for two-dimensional space and q is the normalized distance between particles a and b defined as $q = \frac{r}{h}$.

For the cubic B-spline function, the effective area of support domain is $2h$.

3.1 Continuity equation

The discrete form of the continuity Eq. (3) for particle a is:

$$\frac{d\rho_a}{dt} = \rho_a \sum_b \forall_b \mathbf{v}_{ab}.\boldsymbol{\nabla}_a W_{ab} \tag{11}$$

where $\mathbf{v}_{ab} = \mathbf{v}_a - \mathbf{v}_b$ is the relative velocity of particles a and b. $\nabla_a W_{ab} = \nabla_a W(r_a - r_b, h)$ is the gradient of the kernel function. The kernel gradient normalization is used due to its increased accuracy [38]. The expression for the kernel gradient normalization is:

$$\nabla W_{ab}^c = L(r)\, \nabla w_{ab} \tag{12}$$

where

$$L(r) = \begin{pmatrix} \sum_b \forall_b (x_b - x)\frac{\partial w_{ab}}{\partial x} & \sum_b \forall_b (x_b - x)\frac{\partial w_{ab}}{\partial y} \\ \sum_b \forall_b (y_b - y)\frac{\partial w_{ab}}{\partial x} & \sum_b \forall_b (y_b - y)\frac{\partial w_{ab}}{\partial y} \end{pmatrix}^{-1} \tag{13}$$

3.2 Momentum equation

The particle acceleration from the pressure gradient can be approximated as:

$$\frac{d\mathbf{v}_a{}^{(p)}}{dt} = -\sum_b m_b \left(\frac{p_a}{\rho_a^2} + \frac{p_b}{\rho_b^2}\right)\boldsymbol{\nabla}_a W_{ab} \tag{14}$$

This form ensures linear and angular momentum conversation [39]. Morris et al. [40] suggested an expression for viscous and Laplacian operators. The expression, shown in following Eq. (15), has been applied in Xu et al. [41] for internal flow simulations.

$$(\nabla.\mu\nabla\mathbf{v})_a \approx \sum_b \forall_b \frac{(\mu_a + \mu_b)\, \mathbf{r}_{ab}.\boldsymbol{\nabla}_a W_{ab}}{(r_{ab}^2 + \eta^2)}\, \mathbf{v}_{ab} \tag{15}$$

Where μ is the dynamic viscosity; $\mathbf{r}_{ab} = \mathbf{r}_a - \mathbf{r}_b$ and η is a small value to avoid singular denominator. While this formulation preserves the linear momentum, it does not generally preserve angular momentum. In SPH formulation, the angular momentum conservation properties influence its performance especially in the simulation of violent free surface flows. For This reason, Cleary et al. [42] proposed the new formulation that conserves angular momentums and performs better for turbulent flows:

$$(\nabla.\mu\nabla\mathbf{v})_a \approx \sum_b 8\forall_b \left(\frac{2\mu_a\mu_b}{\mu_a + \mu_b}\right)\frac{\mathbf{r}_{ab}.\mathbf{v}_{ab}}{(r_{ab}^2 + \eta^2)}\, \boldsymbol{\nabla}_a W_{ab} \tag{16}$$

However, Eqs. (15–16) result in many numerical errors around the free surface. By showing the inaccuracy of these relationships in the absence of precise interpolation around free surfaces, Schwaiger [43] expressed the Laplacian of pressure and viscosity term with the suggestion of a new operator:

$$\left(\nabla^2 p\right)_a \simeq \frac{tr\left(\Gamma^{-1}\right)}{n} \left\{ \sum_b 2\forall_b \frac{\mathbf{r}_{ab}.\nabla_a W_{ab}}{\left(r_{ab}^2+\eta^2\right)} p_{ab} - 2\nabla p_a.\left(\sum_b \forall_b \nabla_a W_{ab}\right)\right\} \tag{17}$$

$$(\nabla.\mu\nabla\mathbf{v})_a \simeq \frac{tr\left(\Gamma^{-1}\right)}{n} \left\{ \begin{array}{l} \sum_b 8\forall_b \left(\frac{2\mu_a\mu_b}{\mu_a+\mu_b}\right) \frac{\mathbf{r}_{ab}.\mathbf{v}_{ab}}{\left(r_{ab}^2+\eta^2\right)} \nabla_a W_{ab} \\ - \left[\nabla\left(\mu_a\mathbf{v}_a\right) - \mathbf{v}_a\nabla\mu_a + \mu_a\nabla\mathbf{v}_a\right].\left(\sum_b \forall_b \nabla_a W_{ab}\right) \end{array} \right\} \tag{18}$$

where n is the number of dimensions and Γ is a tensor, defined as:

$$\Gamma_{ij} = -\sum \forall_b \frac{\mathbf{r}_{ab}.\nabla W_{ab}}{\left|r_{ab}^2\right|} r_{ab}^i r_{ab}^j \tag{19}$$

where i and j stand for the coordinate directions, different from a and b for the particles. The gradient calculation in the second term on the right hand side of Eqs. (17) and (18) is corrected through Eq. (12), which can further reduce the error around the free surface [43]. Thus, on applying the above spatial discretizations,the discretized conservation of momentum equation is,

$$\begin{aligned} \frac{d\mathbf{v}_a}{dt} &= -\sum_b m_b \left(\frac{p_a}{\rho_a^2}+\frac{p_b}{\rho_b^2}\right)\nabla_a W_{ab} \\ &+ \sum_b m_b \left(\frac{\tau_a}{\rho_a^2}+\frac{\tau_b}{\rho_b^2}\right)\nabla_a W_{ab} + \mathbf{g} \\ &+ \frac{tr\left(\Gamma^{-1}\right)}{2\rho_a} \left\{ \begin{array}{l} \sum_b 8\forall_b \left(\frac{2\mu_a\mu_b}{\mu_a+\mu_b}\right) \frac{\mathbf{r}_{ab}.\mathbf{v}_{ab}}{\left(r_{ab}^2+\eta^2\right)} \nabla_a W_{ab} \\ - \left[\nabla\left(\mu_a\mathbf{v}_a\right) - \mathbf{v}_a\nabla\mu_a + \mu_a\nabla\mathbf{v}_a\right].\left(\sum_b \forall_b \nabla_a W_{ab}\right) \end{array} \right\} \end{aligned} \tag{20}$$

In the present study, the SPH formulations preserving conservation properties were preferred.

3.3 Boundary treatment

Three layers of dummy particles, called 'boundary particles', are generated in the boundary region parallel to solid wall, to simulate the solid boundary proposed by Morris et al. [40], see Fig. 1. The main advantage of dummy particles is the simplicity of their use in complex geometries, as well as the exact description of the boundary in simulation, when the initial arrangement of particles is performed.

In Fig. 1, The fluid particles near the wall interact with the dummy particles based on their support domain. The distance between the dummy particles is equal to the initial distance between the real particles and the dummy particles are not allowed to move. The viscosity given to the dummy particles is the same as of the real particle, and the fictitious velocity is linearly determined in terms of their distance from the corresponding boundary of the neighboring fluid particle with the following equation:

$$\mathbf{v}_b = -\frac{d_b}{d_a}\mathbf{v}_a \tag{21}$$

The velocity differences are calculated by using the following equation:

$$\mathbf{v}_{ab} = \beta\mathbf{v}_a \tag{22}$$

Where the non dimensional β value is chosen so that:

$$\beta = \min\left(\beta_{\max}, 1+\frac{d_b}{d_a}\right) \tag{23}$$

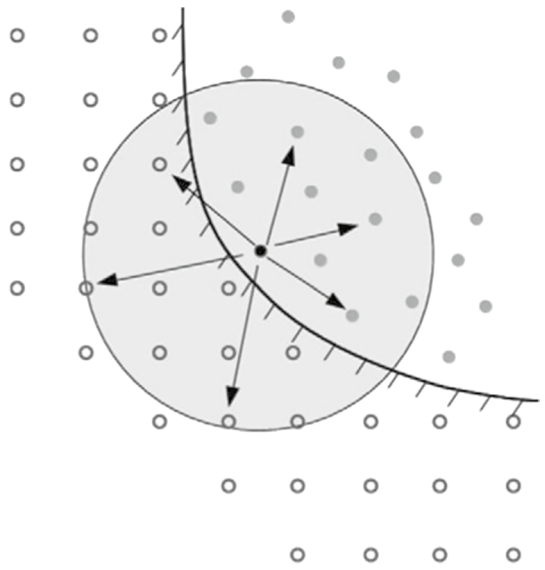

Fig. 1 Fluid particle (•) interact with dummy particles representing the wall (°) to ensure full support of the kernel interpolation

The choice $\beta_{\max} = 1.5$ by Morris et al. [40] led to good results. In this research, good results have also been obtained by choosing $\beta_{\max} = 1.8$.

For the pressure calculation of dummy particles, Adami et al. [44] applied a free-slip wall boundary condition by simply omitting the viscous interaction of a fluid particle with adjacent dummy particles. As shown by Adami et al. [44] the pressure of a stationary dummy particle, w, inspired by a single approaching fluid particle, f, is computed as:

$$p_\omega = p_f + \rho g \left(y_f - y_w\right) \tag{24}$$

The quantities corresponding to dummy and approaching fluid particles are denoted by respective subscripts, hereafter. The second term on the right hand side of Eq. (24) is the hydrostatic component. In the SPH convention Eq. (24) is expressed as:

$$p_\omega = \frac{\sum_f \left[p_f + \rho g \left(y_f - y_w\right)\right] \forall_f W_{\omega f}}{\sum_f \forall_f W_{\omega f}} \tag{25}$$

As we do not update the properties of dummy particles in a wall, we obtain its density from the pressure p_ω:

$$\rho_\omega = \rho_{0,f}\left(\frac{p_\omega}{K} + 1\right) \tag{26}$$

4 Modified SPH algorithm

Using Eq. (14) to determine the pressure gradient leads to the calculation of non-zero pressure gradients for constant pressure fields. Hence, the inaccurate determination of the pressure and the increase of its oscillations will result in a numerical error, especially in free surface regions. Fatehi and Manzari [45] showed that the velocity–pressure coupling reduces the nonphysical fluctuations. In an explicit time-marching scheme, the continuity Eq. (1) to update densities is introduced as:

$$\rho^{n+1} = \rho^n - \Delta t \rho^n \left\langle \nabla . \mathbf{v}^{n+1} \right\rangle \tag{27}$$

The SPH discretization of momentum equation, namely Eq. (2) as an explicit time-marching scheme leads to:

$$\mathbf{v}^{n+1} = \mathbf{v}^n + \Delta t \left[\left\langle -\frac{\nabla p}{\rho} \right\rangle + \nu \nabla^2 \mathbf{v} + \mathbf{g} + \frac{\nabla . \vec{\tau}}{\rho}\right] \tag{28}$$

Thus, The coupling between the velocity of the fluid and the pressure field can be presented as:

$$\begin{aligned}\rho^{n+1} =& \rho^n - \Delta t \rho^n \left\{ \nabla . \left[\mathbf{v} + \Delta t \left(\nu \nabla^2 \mathbf{v} + \mathbf{g} + \frac{\nabla . \vec{\tau}}{\rho}\right)^n\right] \right.\\ & \left. - \Delta t \left[\nabla . \left(\frac{\nabla p}{\rho}\right)\right] \right\}\end{aligned} \tag{29}$$

The pressure fluctuations are prevented by applying a similar approach. To this end, $\nabla . \left(\frac{\nabla p}{\rho}\right)$ in Eq. (29) is substituted by an equivalent term $\frac{\nabla^2 p}{\rho} - \frac{1}{\rho^2} \nabla \rho . \nabla p$. Therefore, using:

$$\mathbf{v}^{n+1} + \Delta t \frac{\nabla p^n}{\rho} = \mathbf{v}^n + \Delta t \left(\nu \nabla^2 \mathbf{v}^n + \mathbf{g} + \frac{\nabla . \vec{\tau}^n}{\rho}\right) \tag{30}$$

The revised form of the semi-discredited continuity equation can be written as:

$$\begin{aligned}\rho^{n+1} =& \rho^n - \Delta t \rho^n \left\{ \nabla . \mathbf{v}^{n+1} + \sigma \Delta t \left(\nabla . \left\langle \frac{\nabla p^n}{\rho} \right\rangle \right.\right.\\ & \left.\left. - \left\langle \frac{\nabla^2 p}{\rho} - \frac{1}{\rho^2} \nabla \rho . \nabla p \right\rangle^n \right) \right\}\end{aligned} \tag{31}$$

In which $\sigma \geq 1$ is a constant. Using this multiplier, one can adjust the amount of correction term to remove the unwanted pressure oscillations in the solution. It is worth noting that

$$\left\langle \nabla . \frac{\nabla p^n}{\rho} \right\rangle_a = \sum_b \forall_b \nabla_a W_{ab} . \left(\left\langle \frac{\nabla p^n}{\rho} \right\rangle_b - \left\langle \frac{\nabla p^n}{\rho} \right\rangle_a \right) \tag{32}$$

The step size is determined according to the stability conditions based on the speed of sound and viscosity [36]:

$$\Delta t < C_{CFL} . \min_a \left(\frac{h_a}{c_a}, 0.1 \frac{\rho_a h_a^2}{\eta_a} \right) \tag{33}$$

where c_a is sound speed of particle a and C_{CFL} is the Courant–Friedrichs–Lewy number, assumed equal to 0.2 for the 2D simulations carried out in the present work.

5 Constitutive law

The relation between pressure and shear stress in one-dimensional problems is written as [13]:

$$\tau = \mu p \tag{34}$$

where the friction coefficient μ depends on, inertial number I, proposed by Da Cruz et al. [13] which is provided by the following equation [14]:

$$I = \frac{|\dot{\gamma}| d}{\sqrt{p / \rho_s}} \tag{35}$$

where $|\dot{\gamma}|$ is the shear strain rate, ρ_s is the density of the grains material, and d is the granular grain diameter. The value of inertial number I, determines the state of the granular flow. For a low inertial number I, the flow is in a quasi-static state with low velocity, and for a very large value of

I, a gaseous regime occurs with high velocity, in which particles do interact with each other [46]. The flow between the quasi-static state and gaseous regime is considered as a viscous or dense state, which the granular material behaves like a fluid. In the dense state, the friction coefficient μ is locally determined by the inertial number I, and satisfies the following equation proposed by Jop et al. [14]:

$$\mu(I) = \mu_s + \frac{\mu_2 - \mu_s}{1 + {}^{I_0}/_{I}} \tag{36}$$

where μ_s and μ_2 are material-dependent parameters. A 2D or 3D equation has been extended by Jop et al. [14] based on the constitutive law in Eq. (34) for the granular material, as following:

$$\tau^{\alpha\beta} = 2\frac{\mu(I)\,p}{|\dot{\gamma}|}\,\varepsilon^{\alpha\beta} = 2\eta\varepsilon^{\alpha\beta} \quad , \quad \eta = \frac{\mu(I)\,p}{|\dot{\gamma}|} \tag{37}$$

In this rheology model, the viscosity is locally determined by the pressure p, inertial number I, and the shear rate $|\dot{\gamma}|$. Based on extensive experimental data and analysis, we have:

$$\eta = \frac{\mu_s p}{|\dot{\gamma}|} + \frac{(\mu_2 - \mu_s)p}{|\dot{\gamma}| + \xi\sqrt{p}} \tag{38}$$

where $\xi = I_0\left(\rho_s D^2\right)^{-0.5}$. In Eq. (38), the first term of the right side represents the yield stress which distinguishes the solid-like and viscous-like flow regimes while the second term can be considered as the stress generated by the visco-plastic behavior of a non-Newtonian fluid. When the viscosity provided by the constitutive equation approaches to infinity, time step of Eq. (33) tends to zero, in these cases, a regularization method is needed to replace the large values of viscosity with small ones, to prevent the undesirable small time steps. The proposed regularization method, inspired from the Papanastasiou's regularization [47] transposed to the $\mu(I)$ rheology:

$$\eta = \mu_s p\,\frac{1 - \mathrm{e}^{-|\dot{\gamma}|/\alpha_r}}{|\dot{\gamma}|} + \frac{(\mu_2 - \mu_s)p}{\xi\sqrt{p} + |\dot{\gamma}|}\cdot\frac{|\dot{\gamma}|}{\sqrt{|\dot{\gamma}|^2 + \alpha_s^2}} \tag{39}$$

where $\alpha_r = 0.01$ and $\alpha_s = 0.000001$. The viscosity profile is shown in Fig 2.

6 Numerical verification and applications

The proposed SPH method coupled with μ(I) local rheology model is applied in modeling glass beads and sand granular flows. The model is first verified by applying it to free-surface granular flowing down an inclined plane. The numerical results can be compared to analytical predictions and experimental data. Subsequently, the proposed algorithm is applied to simulate granular column collapses for different column ratios and granular dam-breaking flows in rectangular channels. Numerical results are compared with different experimental observations.

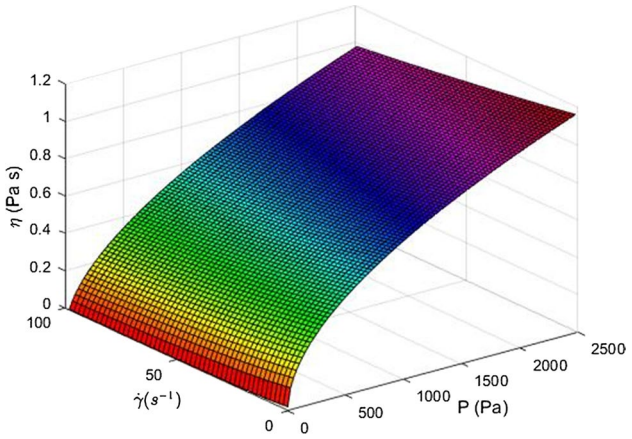

Fig. 2 The variation of viscosity versus the pressure and the shear rate

6.1 Granular flow on an incline

We first consider a two-dimensional steady incompressible granular layer with thickness h, of the granular material of solid fraction φ defined as $\varphi = \frac{\rho}{\rho_s}$ composed of grains of diameter d along an infinite plane inclined at an angle θ. The analytical solution is the so-called Bagnold's profile where the frictional granular shear stress is modeled using the μ(I) rheology [48]. The steady-state velocity profile of the solution has the following expression [49]:

$$\frac{U(y)}{\sqrt{gd}} = \frac{2}{3}\,\bar{I}\sqrt{\varphi\,\cos\theta}\;\frac{\left[h^{3/2} - (h-y)^{3/2}\right]}{d^{3/2}} \tag{40}$$

For this velocity profile, the mean velocity $\bar{U}$ and the mean inertial number $\bar{I}$ are defined respectively by:

$$\bar{I} = \frac{5}{2}\frac{\bar{U}d}{h\sqrt{\varphi g h\cos\theta}} \quad , \quad \bar{U} = \frac{3}{5}U(h) \tag{41}$$

where $U(h)$ is the free surface velocity. Since the depth-averaged velocity $\bar{U}$ is the same everywhere, equal to U_0. It is possible to determine it by using Eq. (40). In each point of the front, the velocity U_0 is:

$$U_0 = \frac{2I_\theta}{5}\sqrt{\varphi g h_s\cos\theta}\frac{h_s}{d} = \frac{2\bar{I}}{5}\sqrt{\varphi g h\cos\theta}\frac{h}{d} \tag{42}$$

where $\bar{I}$ and I_θ are the inertial numbers associated with the flow of thickness h and the steady-uniform flow of thickness

h_s far upstream respectively. In fact, the function $h_s(\theta)$ is the thickness of the deposit left by a steady uniform flow at the inclination θ. The Eq. (43) is the relationship between $\bar{I}$ and I_θ:

$$\frac{I_\theta}{\bar{I}} = \left(\frac{h}{h_s}\right)^{3/2} \tag{43}$$

In the steady-uniform flow, the Eq. (36) can be expressed as a function of I_θ by using the friction law:

$$\tan\theta = \mu(I_\theta) = \mu_s + \frac{\mu_2 - \mu_s}{1 + {}^{I_0}/_{I_\theta}} \tag{44}$$

The Eqs. (43) and (44) allow us to replace ${}^{\bar{I}}/_{I_0}$ with a function of ${}^{h}/_{h_s}$:

$$\frac{\bar{I}}{I_0} = \left(\frac{h_s}{h}\right)^{3/2} \frac{\tan\theta - \mu_s}{\mu_2 - \tan\theta} \tag{45}$$

During experiments with granular material released down an inclined plane, the mean velocity $\bar{U}$, the inclination θ and the thickness h were related through the following experimental relation [50]:

$$\frac{\bar{U}}{\sqrt{gh}} = -\gamma + \beta\frac{h}{h_s(\theta)} \tag{46}$$

where γ and β are empirical parameters which depend on the material. Jop et al. [48] found the following expression for the parameter I_0 of Eq. (36):

$$I_0 = \frac{5}{2}\frac{\beta\, d}{L\sqrt{\varphi\cos\theta}} \tag{47}$$

where L is a constant parameter which depends on the material. In the constitutive law, I_0 should be a constant, whereas it depends on θ through the term $\sqrt{\cos\theta}$. However, this term does not vary much in the experimental range.

The values for parameters L,γ,β,μ_s,μ_2 from experimental measurements obtained by Forterre and Pouliquen [50] are listed in Table 1.

For glass beads with $\gamma = 0.0$ by using Eqs. (41) and (46), we obtain an empirical relation for $\bar{I}$:

$$\bar{I} = \frac{5}{2}\frac{\beta\, d}{\sqrt{\varphi\cos\theta}}\frac{1}{h_s} \tag{48}$$

By using Eqs. (45), (47) and (48), one finds that h_s should be related to inclination θ and thickness h through the relation:

$$h_s^{5/2} = L.h^{3/2}\,\frac{\mu_2 - \tan\theta}{\tan\theta - \mu_s} \tag{49}$$

Table 1 Parameters for the rheology model [50]

	Glass beads (d = 0.5 mm) †	Sand (d = 0.8 mm)
${}^{L}/_{d}$	1.65	2.03
γ	0.0	0.77
β	0.136	0.65
μ_s	tan(20.9°)	tan(27.0°)
μ_2	tan(32.76°)	tan(43.4°)

† For glass beads by taking $\varphi \approx 0.6$ and an average value of $\theta = 25°$, $I_0 = 0.279$

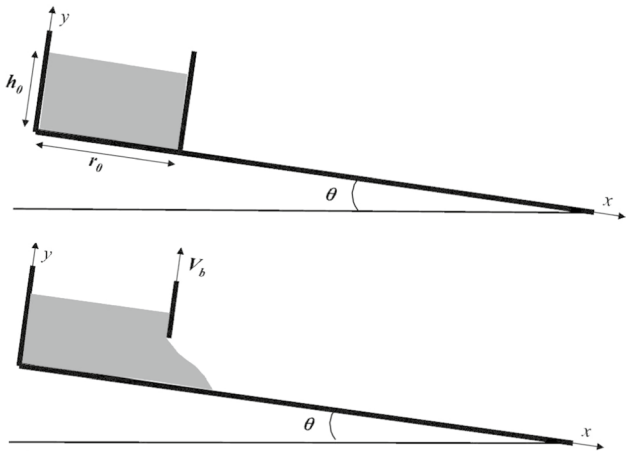

Fig. 3 Experimental setup: The initial mass (light gray) with initial thickness $h_0 = 14$ cm and width $r_0 = 20$ cm is released on a plane with inclination θ by opening a gate with constant speed. [7]

In steady state, by setting the boundary condition $h = h_s = const.$ far upstream to the front, the Eq. (49) is simplified to the following form:

$$h_s = L\frac{\mu_2 - \tan\theta}{\tan\theta - \mu_s} \tag{50}$$

To validate the proposed algorithm and local pressure-dependent viscosity, we will simulate here, the collapse of granular columns over inclined channels and compare results with experimental one [7]. The experimental set-up consists of a planar channel with 3m length with possible inclination angles θ varying from horizontal up to 25.0°. A rectangular granular mass of thickness $h_0 = 14$ cm and of downslope length $r_0 = 20$ cm , an aspect ratio $a = h_0/r_0 = 0.7$ is released gradually from a reservoir at time $t = 0.s$ by opening a gate (Fig. 3).

The glass beads are sub-spherical, cohesion-less and highly rigid with a diameter $d = 0.5$ mm. They flow down an inclined channel, roughened by gluing a layer of the same beads on its surface. The particle density $\rho_s = 2500\,\mathrm{kg\,m^{-3}}$ and volume fraction $\varphi = 0.6$ of the

mass were estimated, giving an apparent flow density of $\rho = \varphi\rho_s = 1500\,\mathrm{kg\,m^{-3}}$. In the experiments, a gate is removed at the initial time to release the granular mass. The gate removal is simulated here by considering a lifting velocity $V_{gate} = 1.3\,\mathrm{ms^{-1}}$as measured in the simulations. To compare flows with different inclinations, the velocity profile and the deposit of thickness are used in the analysis. Steady granular flows are observed in all the tested inclinations in numerical simulation. The velocity profiles are given in Fig. 4. The analytical solutions in Sect. 6.1 are used as the reference. Fig. 4 shows the validation of the numerical model against the Bagnold analytical solution regarding stream wise velocity profiles. For all three inclinations, the good agreement is obtained with respect to the analytical solution.

The granular bed has been created by the deposit of steady uniform flows in the inclined plane. Indeed, thin, steady uniform granular flows can be observed within a range of inclination angles [6]. These flows leave a uniform deposit along the plane with a thickness h_s. The variation of $\frac{h_s}{d}$ vs. θ is shown in Fig. 5. Here h_s represents the minimum thickness for flow at a given angle θ [6]. The experimental results [6] are well-fitted by Eq. (50). Also, the numerical results are in good agreement with experimental data.

The collapse of granular mass is simulated on a gentle slope using similar parameters. Granular mass is in contact without friction with a gate; the gate is removed in the direction perpendicular to the inclined bed. The simulation with the regularized constitutive law (Eq. (39)) is shown in Fig. 6.

The collapse of the mass at the top of the channel is very fast, and the progressive front also goes faster than the experimental model. Except for run-out distances, the final form of the deposit is comparable to the experimental results.

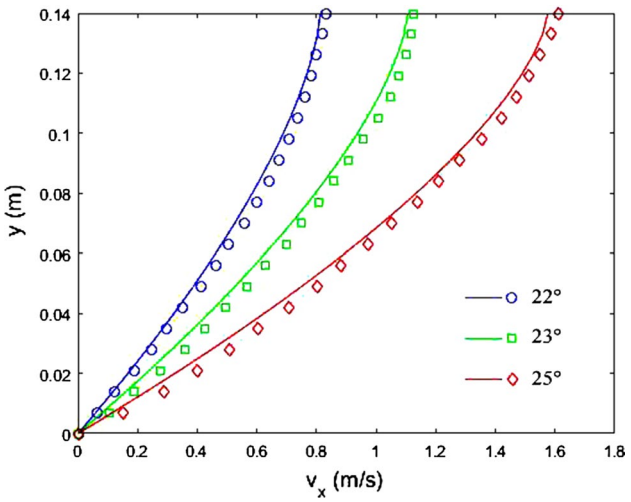

Fig. 4 Velocity profiles: lines indicate reference solutions calculated from Eq. (40) and markers are numerical results

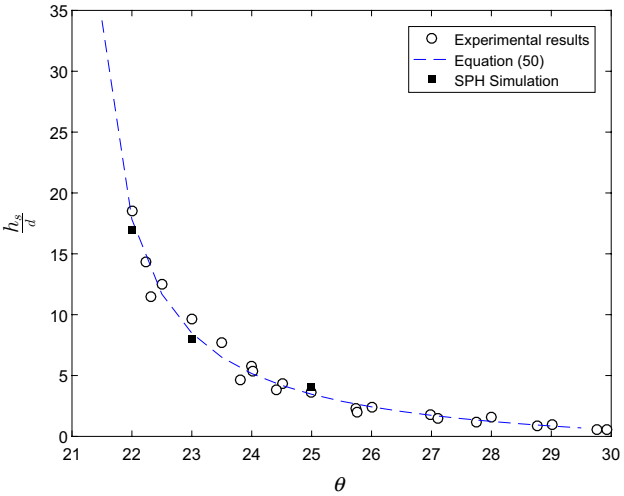

Fig. 5 Thickness h_s left on a plane of inclination angle θ after steady uniform flows

Considering the actual effect of bed friction at $\theta = 22°$ would lead to further progress, a better fit with empirical results will be observed. The maximum flowing thickness is about 5 cm for $\theta = 22°$. These results are in good agreement with the simulations of flows over an inclined plane performed by Mangeney et al. [7].

At the instant $t = 0.11$cm, just after the gate is removed, which triggers a near bed flow. the maximum horizontal velocity is obtained close to the substrate. In the following, the flow is concentrated only in a shallow sub-domain close to the free surface which is observed with the velocity field. The maximum horizontal velocity is obtained near the free surface. In the flowing region, the horizontal velocity has a parabolic profile similar to Eq. (40) (Fig. 6c).

The viscosity value can be obtained from Eq. (38) only with the initial thickness of the column h_0, the diameter and grain density, the slope angle and the rheological parameters. The amount of pressure, assuming that the flow layer has a thickness equal to half the initial thickness, determines the viscosity $\eta \simeq 1.4$ pa s. Note that, for this calculation, the strain rate in Eq. (38) is negligible.

As observed in Fig. 7, in the flowing region, the viscosity gradually increases with the distance perpendicular to the free surface, which seems to be mainly influenced by the increased pressure. The viscosity near the transition of the static/flowing region is slightly lower than its value for the collapse on the horizontal bed. The viscosity decreases towards the front where it is less than 0.7 pa s. The viscosity changes between the maximum value in the static region and its minimum value, which is obtained in the vicinity of the forward and near the free surface. As a result, the viscosity mainly shows a pattern similar to the pressure field, which covers the effect of the strain rate.

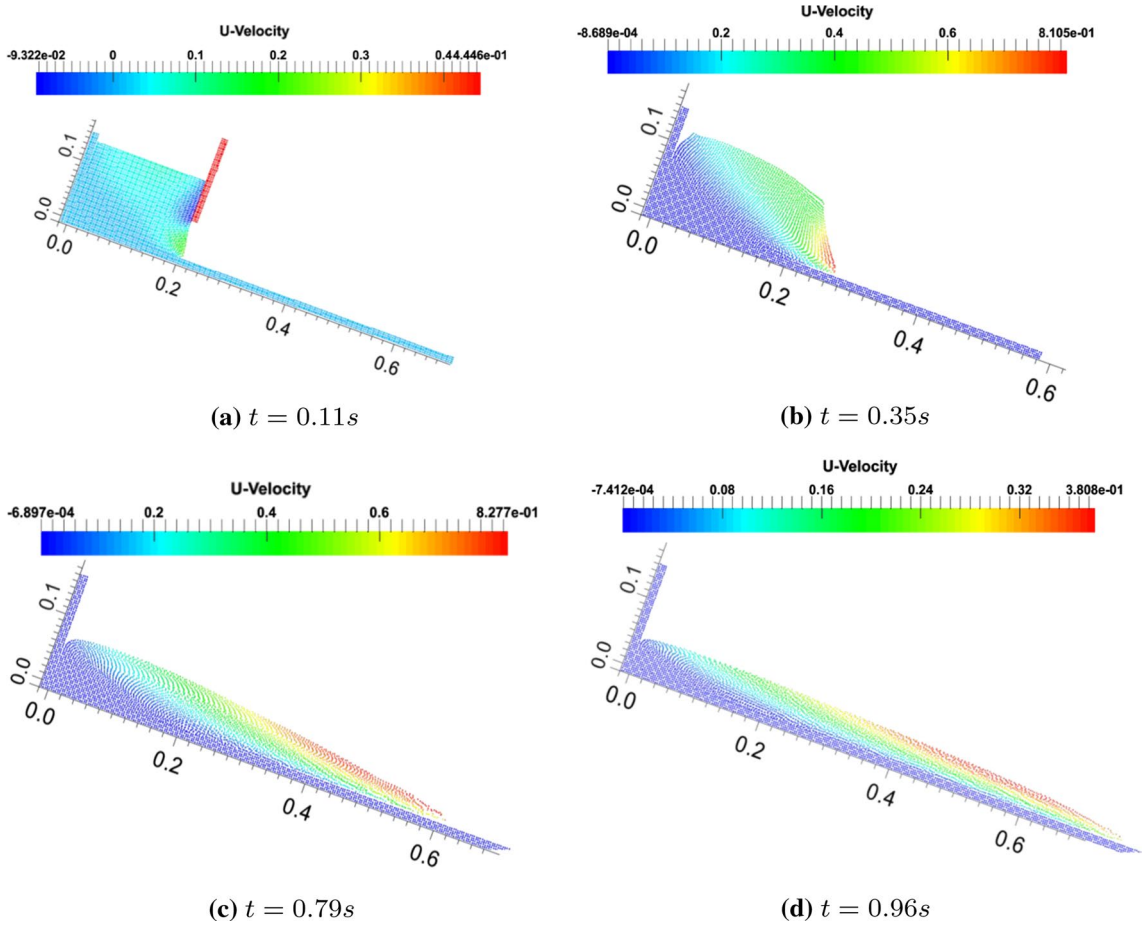

(a) $t = 0.11s$ **(b)** $t = 0.35s$

(c) $t = 0.79s$ **(d)** $t = 0.96s$

Fig. 6 Snapshots of the granular collapse over a plane inclined at $\theta = 22°$. The colors represent the distribution of Horizontal velocity

The distribution of the strain rate is an interesting feature. High strain rate zone is concentrated initially near the bed close to the front and further upslope along most of the flowing region.

Figure 8 shows the comparison of the simulated granular mass and the experimental results performed by Mangeney et al. [7] at different times for thickness profile as a function of the down slope during the collapse for inclination angle $\theta = 10°$. Obviously, as the angle increases, the deposit extends further down the plane and becomes flatter. In the initial stage, the flow is observed lagging behind the experimental results (Fig. 8a). The shape of the final deposit is in good agreement with the laboratory results, except in the vicinity of the back wall, where the simulated maximum thickness is smaller, and the front is running slower, the final run-out distance is about 15% shorter than experimental results, The viscous effects strongly change the flow dynamics and deposit so the dissipation due to plastic deformation is much smaller than that due to viscous effects. The viscosity of the lateral wall should be several times higher than the viscosity of granular media. Therefore, by considering the actual effect of the viscosity of the wall, the thickness of the deposit near the back wall increases, which it match the experimental observations.

6.2 The granular column collapse

The collapse of the confined column of grains onto a horizontal plane under its own weight is known as "granular column collapse" which starts with the vertical fall of grains alongside lateral spreading flow; . The focus is on the scaling law corresponds to the final distance of the flow front, which is called run-out distance. The experiment was performed in quasi-two dimensions configuration by Lajeunesse et al. [1] and Lube et al. [4]. If the initial height of the column is h_0, its initial half-width is r_0, the final maximum thickness is h_∞ and the final half-width is r_∞ (Fig. 9).

The experimental scaling for the run-out distance in the two-dimensional configuration reads:

$$\frac{r_\infty - r_0}{r_0} \simeq \begin{cases} \lambda_1 a, & a < a_0 \\ \lambda_2 a^\beta, & a > a_0 \end{cases} \tag{51}$$

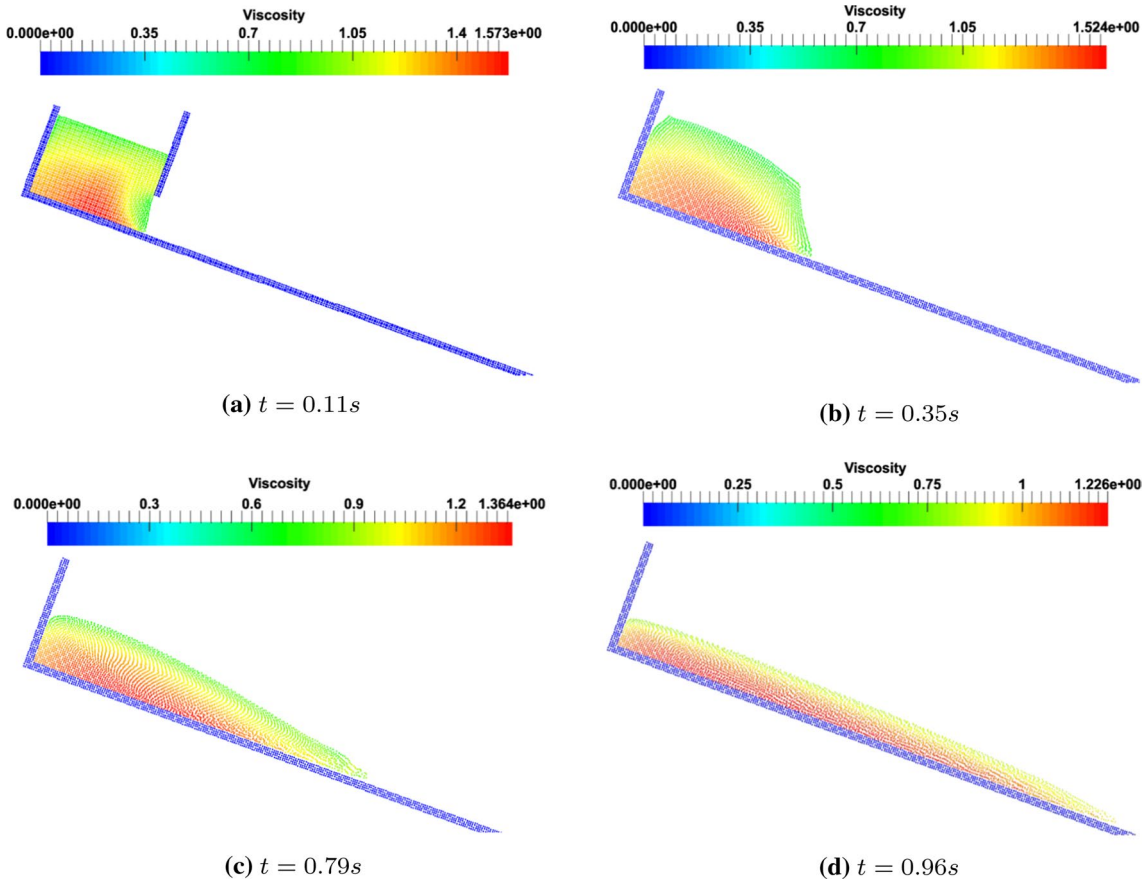

(a) $t = 0.11s$ **(b)** $t = 0.35s$ **(c)** $t = 0.79s$ **(d)** $t = 0.96s$

Fig. 7 Viscosity (in Pa s) calculated with the $\mu(I)$ rheology at different times for granular collapse over a plane inclined at $\theta = 22°$

Where $a = h_0/r_0$ is the column aspect ratio and λ_1, λ_2, β, a_0 are essentially material dependent parameters. In two dimensions, Lube at al. [4] found $\lambda_1 \simeq 1.2$, $\lambda_2 \simeq 1.9$, $\beta \simeq {}^2/_3$ and $1.8 \leq a_0 \leq 2.8$ for sand and sugar. Lube et al. [4] found a small transitional region for $1.8 \leq a_0 \leq 2.8$ between the linear and the power-law descriptions which is shown in Fig. 13, while Lajeunesse et al. [1] found $\lambda_1 \simeq 1.8$, $\lambda_2 \simeq 2.3$, $\beta \simeq {}^2/_3$ and $a_0 \simeq 3.0$ for glass beads. Similar scaling was obtained for the final height of the deposit:

$$\frac{h_\infty}{r_0} \simeq \begin{cases} \lambda_3 a, & a < a_0 \\ \lambda_4 a^\kappa, & a > a_0 \end{cases} \tag{52}$$

Where Lube et al. [3] found $\lambda_3 \simeq 1.0$, $\lambda_4 \simeq 1.0$, $\kappa \simeq 0.4$ and $a_0 \simeq 1.15$. To follow the experimental set-ups, the parameters of rheology model as shown in Table 2. are used in simulation for initial column ratios $0.19 \leq a \leq 3.0$, with the initial radius $r_0 = 97.2$ mm, and for $a > 3.0$, $r_0 = 29.2$ mm. The solid density $\rho_s = 2600\,\mathrm{Kgm}^{-3}$ and the volume fraction is set to be 0.62. We note that the time of each experiment depends only on the height of the initial column of the mass of the grains and follows the relation [1]:

$$t_s \simeq 3.2\sqrt{\frac{h_0}{g}} \tag{53}$$

The sand and glass beads collapse simulations of the granular column show that the rheological model in SPH can determine the characteristics of granular flow in a dense state. The granular media behaves like a fluid at the beginning of the movement. During the flow, it gradually becomes a quasi-static state with lower velocity and less mobility. The displacement and failure mechanism of the granular flow column can be affected by many factors such as grain size, granular material, and roughness of the bed. To demonstrate the granular flows clearly, Figs. 10, 11 and 12 show three granular column failure flows of sand for $a = 0.9$, $a = 2.75$ and $a = 4.8$. Two patterns of flow for the collapse of the granular column can be seen in Figs. 10, 11 and 12. In the collapse process, the column on both sides begins to move in the outward direction, because the surface particles that slip on the substrate become less and less, the column gradually reaches its final deposit.

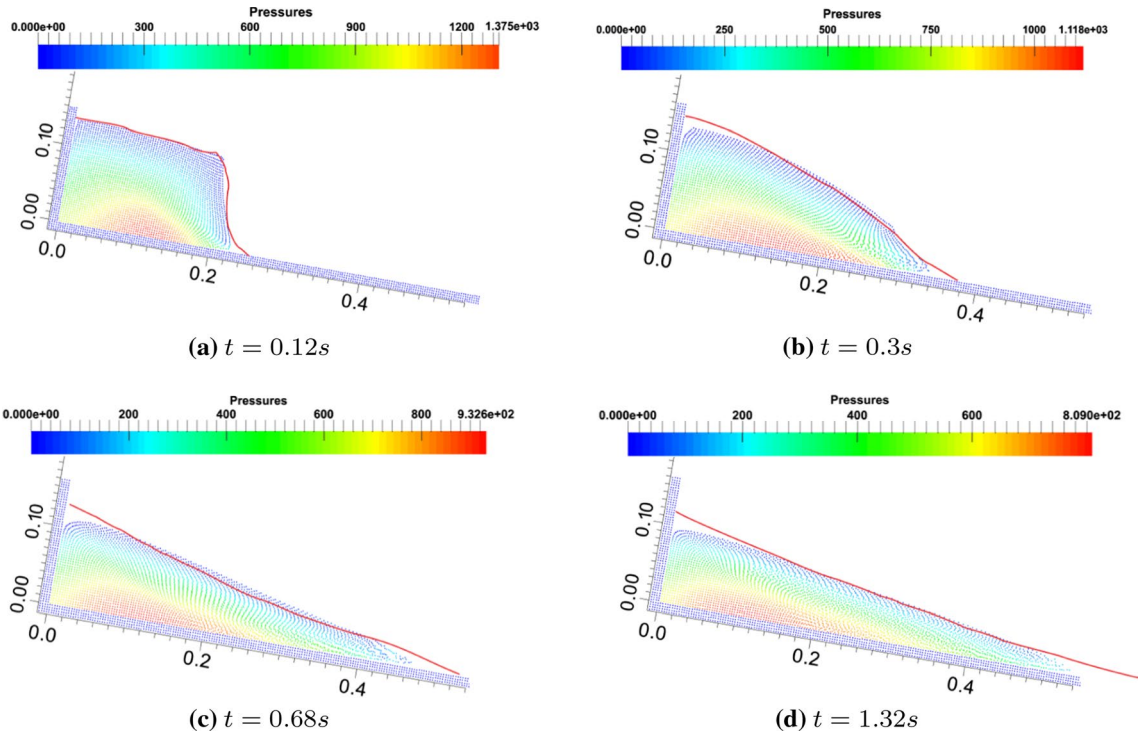

Fig. 8 Comparison of the simulated granular mass and the experimental results (pink line) at different times for granular collapse over a plane inclined at $\theta = 10°$: the colors represent the distribution of pressure (pa) (color figure online)

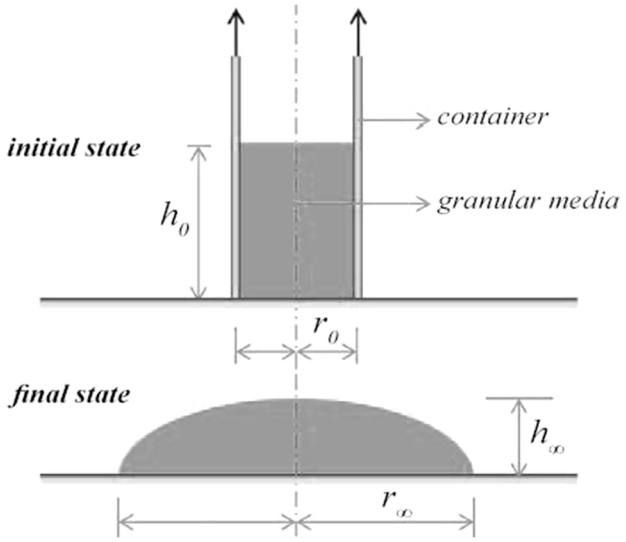

Fig. 9 Granular columns collapse: sketch of experimental set-up and parameters definition [4]

Table 2 Parameters reology for sand column collapse [48]

	μ_s	μ_2	I_0
Sand (d=0.32 mm)	tan(30.5°)	tan(51.3°)	2.65

In Fig. 10, particles of fronts move outwards and large velocity can be observed at both sides of the column fronts at $t = 0.05$ s. At $t = 0.07$ s, more particles on the free surfaces extend over the horizontal bed to the outwards, because the particles fall off the top of the column at high velocity. The shape of the column is changing to a sinusoidal function since it moves symmetrically and simultaneously in both directions. In the time of particles spreading from the surface, high-velocity particles are gradually approaching from the flow state to the quasi-static state. As a result, there are fewer flowing particles with high velocity on the surface at $t = 0.11$ s (Comparing with those at $t = 0.1$ s). So, the proposed model results in a lower velocity of spreading, thus less displacement of the front, which is in better match with the experiments.

For ratio $a = 2.75$, the collapse of column begins from both sides with sliding down the surface particles to the substrate as demonstrated in Fig. 11b–c. A cone deposit of the column is left (Fig. 11d).

For the column ratio, $a = 4.8$, the upper part of the column retains its original shape, falls in the vertical direction; Beside both sides of the front, the particles are gradually deviating horizontally, so the particles collide vertically with static particles in the center as shown in Fig. 12a at $t = 0.03$ s, After the column collapses completely, the flow is similar to that for $a = 2.75$. For a much

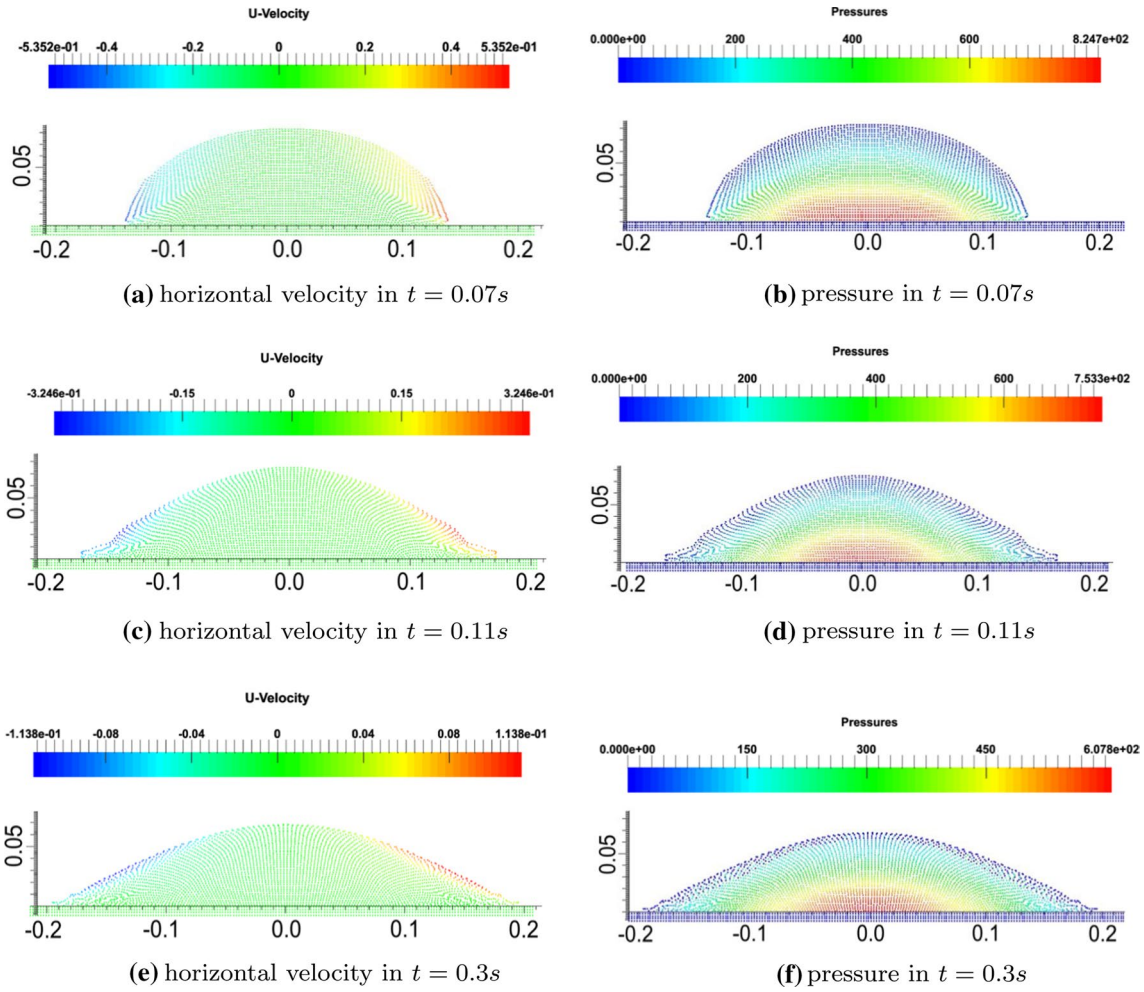

Fig. 10 horizontal velocity (ms^{-1}) (left column) and pressure (Pa) (right column), calculated with variable viscosity with the $\mu(I)$ rheology at different times for granular collapse over a horizontal plane for $a = 0.9$

larger column, $a = 4.80$ (Fig. 12), the falling process of the upper part is more obvious in Fig. 12a, and even at $t = 0.1$ s, this part is still observed in Fig. 12b.

Figure 13 shows that a good agreement exists between numerical and experimental results [3, 4] indicating that the proposed SPH model is able to correctly simulate this kind of granular flow.

6.3 Granular dam-breaking flows

In this section, the SPH method is applied to model rectangular pile of granular material that allows a dam-breaking flow to be produced in channels. The model set-ups follow the experiments conducted by Lajeunesse et al. [1, 2]. The particles are arranged in a square lattice with an initial separation of 1 mm, and thus smoothing length of 1.3 mm. Also, three layers of SPH particles are located outside the computational granular domain to represent the solid wall. It is used to model dam-breaking flows caused by glass beads.

The density is $\rho_s = 2600\,\mathrm{Kgm}^{-3}$; the volume fraction is set to be 0.62 according to the experiments by Lajeunesse et al. [1, 2]. In this study, the flows in simulations are performed in two dimensional configurations. Similar to the cylindrical column failure, the initial ratio $a = h_0/l_0$ is important in spreading of the granular materials in the channel. Lajeunesse et al. [1] observed at small a, the flow is initiated by failure at the edge of the pile along the upper surface where material slides down, on the other hand, Underlying grains remain static. when the flow is developed, the velocity profile in the vicinity of the front, is in the horizontal direction (Fig. 14).

The ratio $a = 0.6$ with initial length $l_0 = 102\,\mathrm{mm}$ was firstly modeled. The velocity vectors of the flows are shown in Fig. 15 for $a = 0.6$. A sliding interface can be defined to distinguish the static internal part and the flowing region; then the interface is added to the simulation

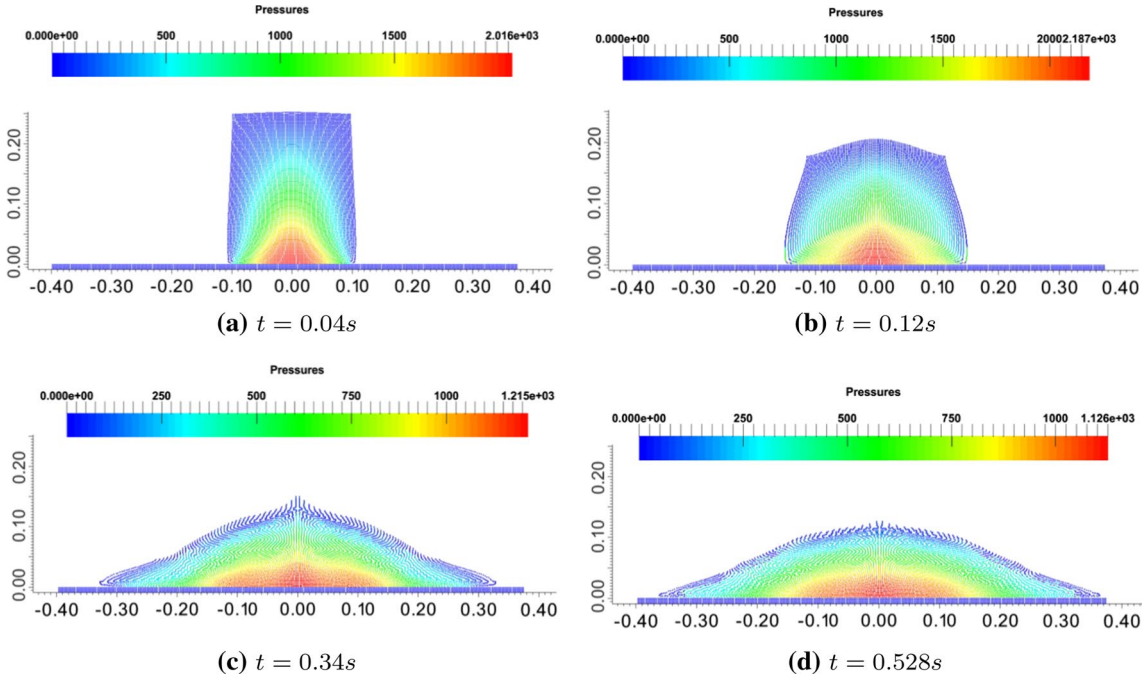

Fig. 11 Values of the pressures (pa) in the model at different times for granular collapse for $a = 2.75$

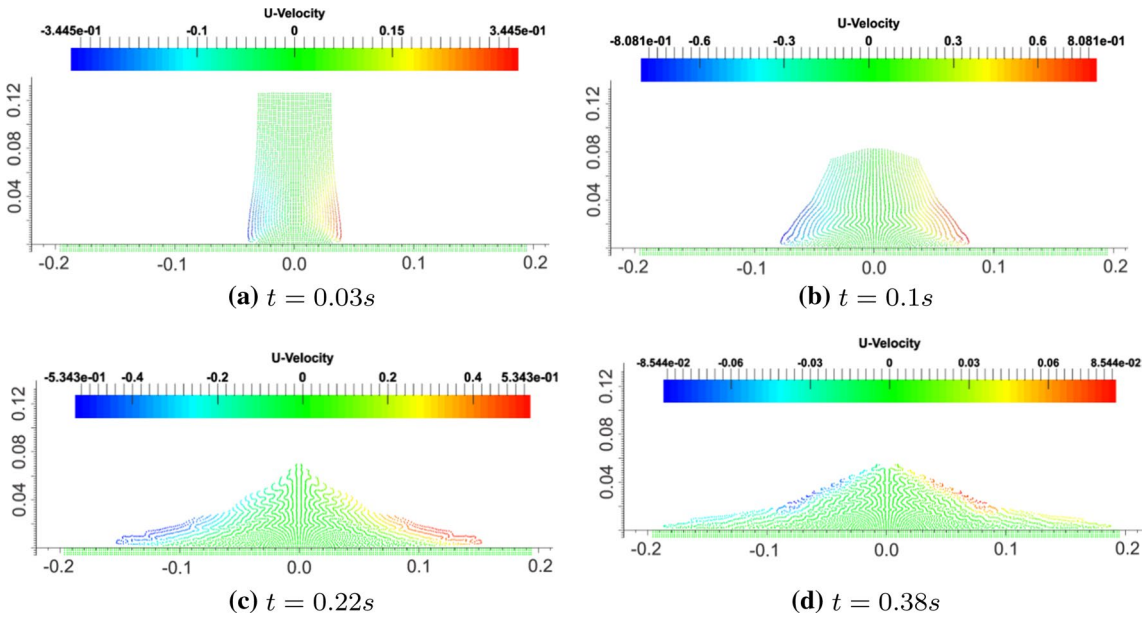

Fig. 12 Values of the horizontal velocity (ms^{-1}) in the model at different times for granular collapse for $a = 4.8$

results to separate the two sections. For a small ratio $a = 0.6$, the collapse of the edge as a granular dam-breaking flow extends along the sliding interface. The velocity near the flow front becomes very high in the whole thickness with the development of the collapse mechanism at $t = 0.07$s. In the distance from the flowing front, high velocity values are available only for particles below the free surface, and then gradually decreases to the sliding interface.

For a large ratio, $a = 3.2$ with the initial length $l_0 = 53$ mm, at $t = 0.02$ at the beginning of the flow, the upper part of the column falls due to gravity in the vertical

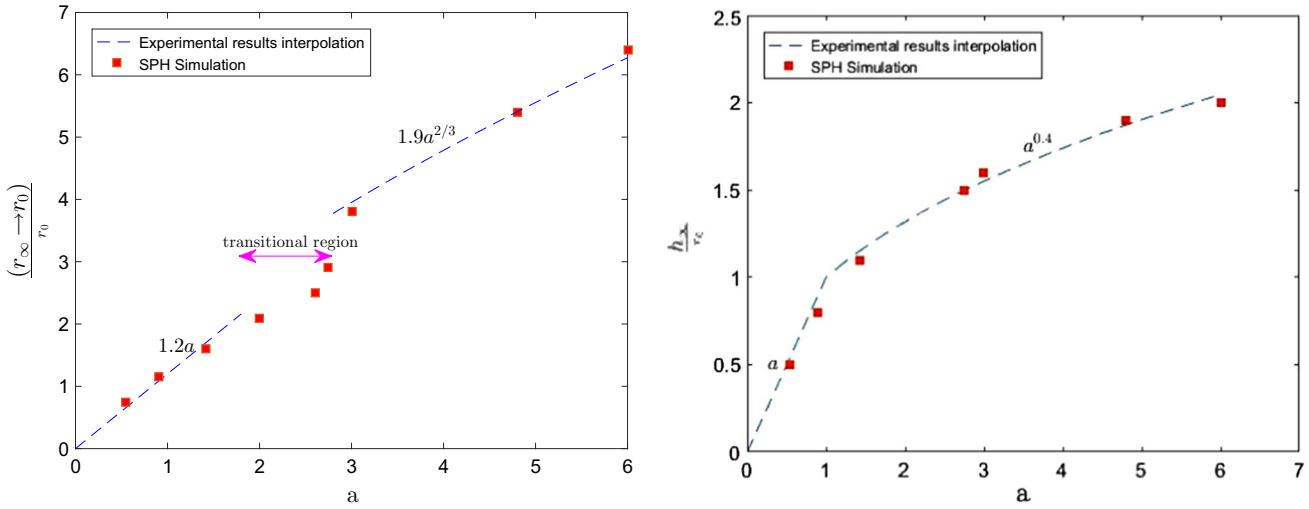

(a) run-out distance **(b)** maximum thickness

Fig. 13 Scaling from numerical simulation compared with scaling from Lube et al. [4] for granular columns collapse

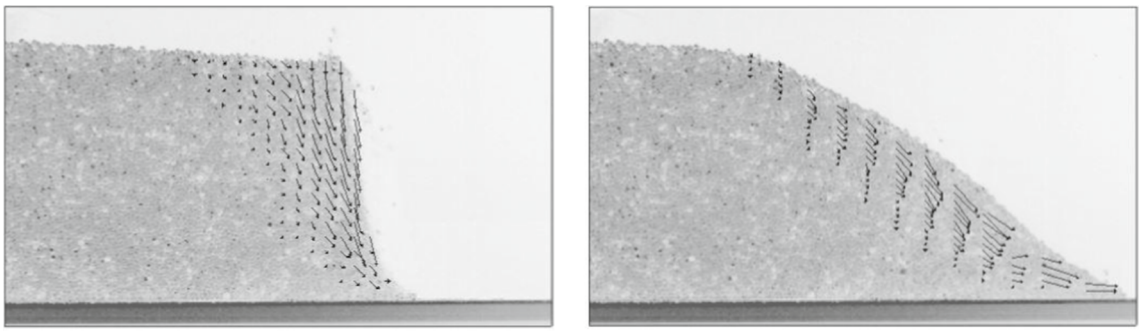

(a) t=0.03s **(b)** t=0.09s

Fig. 14 Velocity field at the wall of the rectangular channel for a = 0.46 [1]

direction, so the vertical velocity in the flowing region is almost the same. In the vicinity of the sliding interface, the velocity vectors diverge gradually in the horizontal direction. After the full collapse of the column at $t = 0.229$ s, the column takes the shape of a triangle. In the vicinity of the front, the flow continues with relatively high velocity vectors. These phenomena are well replicated in simulations compared to experimental results (Fig. 16).

Figure 17 shows the evolution of the mass front $(l - l_0)/l_0$ with time for $a = 0.6$, where the time is scaled with $\tau_c = \left(h_0/g\right)^{0.5}$. The experimental results [1, 2] are also plotted in the figure for comparisons. After passing the transient acceleration stage, which lasts approximately $0.8\tau_c$, the pillar base moves at the approximately constant spreading velocity for about $0.2\tau_c$. Most of the total distance traveled by the pillar base takes place within this time interval. Eventually, the advance front slows down and stops at about $0.6\tau_c$. The front movements in this period almost follow an inclined line with a constant slope.

7 Discussion

In this study, the numerical results presented using a visco-plastic-based constitutive law in SPH framework, express the dynamic behavior of granular free-flow flows. In other words, as observed in the experiments, the formation of a uniform region and the flow-transfer property were well reproduced. In the collapse of the granular column on inclined bed simulation, the results confirm that the uniform region behind the flow front behaves as a steady uniform regime with a Bagnold velocity profile and numerical parameters, in addition to having a small effect on the final deposit, play an important role in the velocity to reach a uniform steady state. Numerical simulations show that the

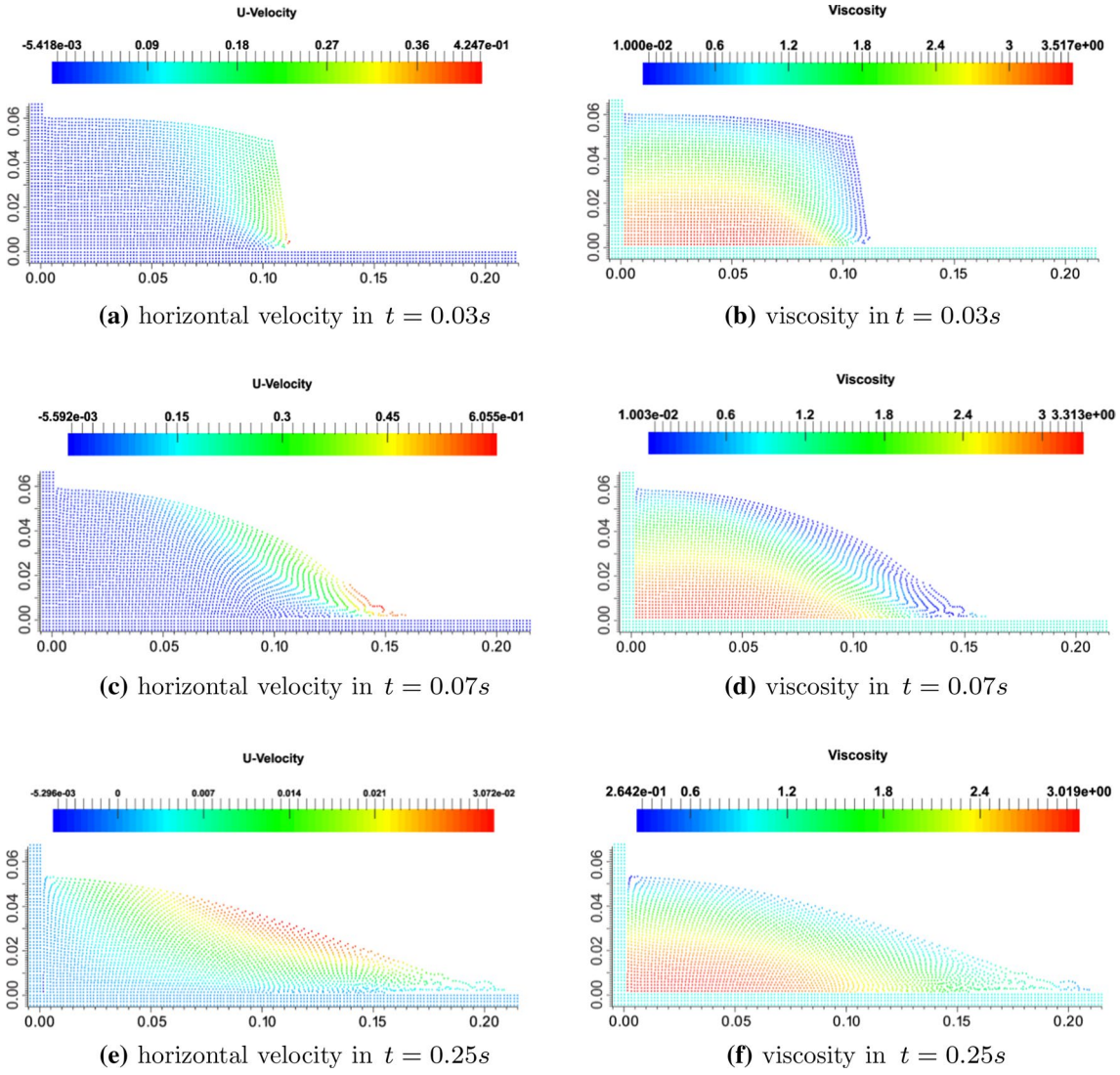

(a) horizontal velocity in $t = 0.03s$ **(b)** viscosity in $t = 0.03s$

(c) horizontal velocity in $t = 0.07s$ **(d)** viscosity in $t = 0.07s$

(e) horizontal velocity in $t = 0.25s$ **(f)** viscosity in $t = 0.25s$

Fig. 15 horizontal velocity (ms^{-1}) (left column) and pressure (Pa) (right column), calculated with variable viscosity with the $\mu(I)$ rheology at different times for granular dam-breaking for $a = 0.6$

viscosity decreases from values greater than $\eta = 1.5$ pa s in deep-static regions to zero in near the free surface. As the angle of substrate increases, the used model predicts the velocity field and run-out distances slightly less than the experimental results. The Simulations show that the main differences are near the front flow and lateral back wall. Indeed, the parameter I of the $\mu(I)$ rheology varies mainly in the flowing region. The thin layer flows over a rigid bed characterize the region near the flow front. The high strain rate regions at the tip of the front are located near the bed. These high deformation regions confirm the strong nonlinear character of the $\mu(I)$ rheology. The considering the actual effect of the viscosity of the wall, it will reduce the overestimated dissipation near the back wall. On the other hand, simulations show that there is the overestimated collapse of the columns near the back wall due to significant sliding of the mass in this region. The velocity profile with the maximum value at the free surface is accompanied by an exponential decrease in velocity near the transition between the flowing and the static regions.

For the granular collapses, In comparison with the experiments, the SPH method with pressure-dependent rheology predict fairly well the time evolution of surface deformation of the granular column after collapsing. The results of the granular column collapse showed that the initial column ratio plays an important role in the granular expansion in the horizontal plane. The difference in the failure mechanism between small values of initial column ratio and high initial column ratios observed in the experiments can also be captured in the SPH simulations. For small column ratios, the

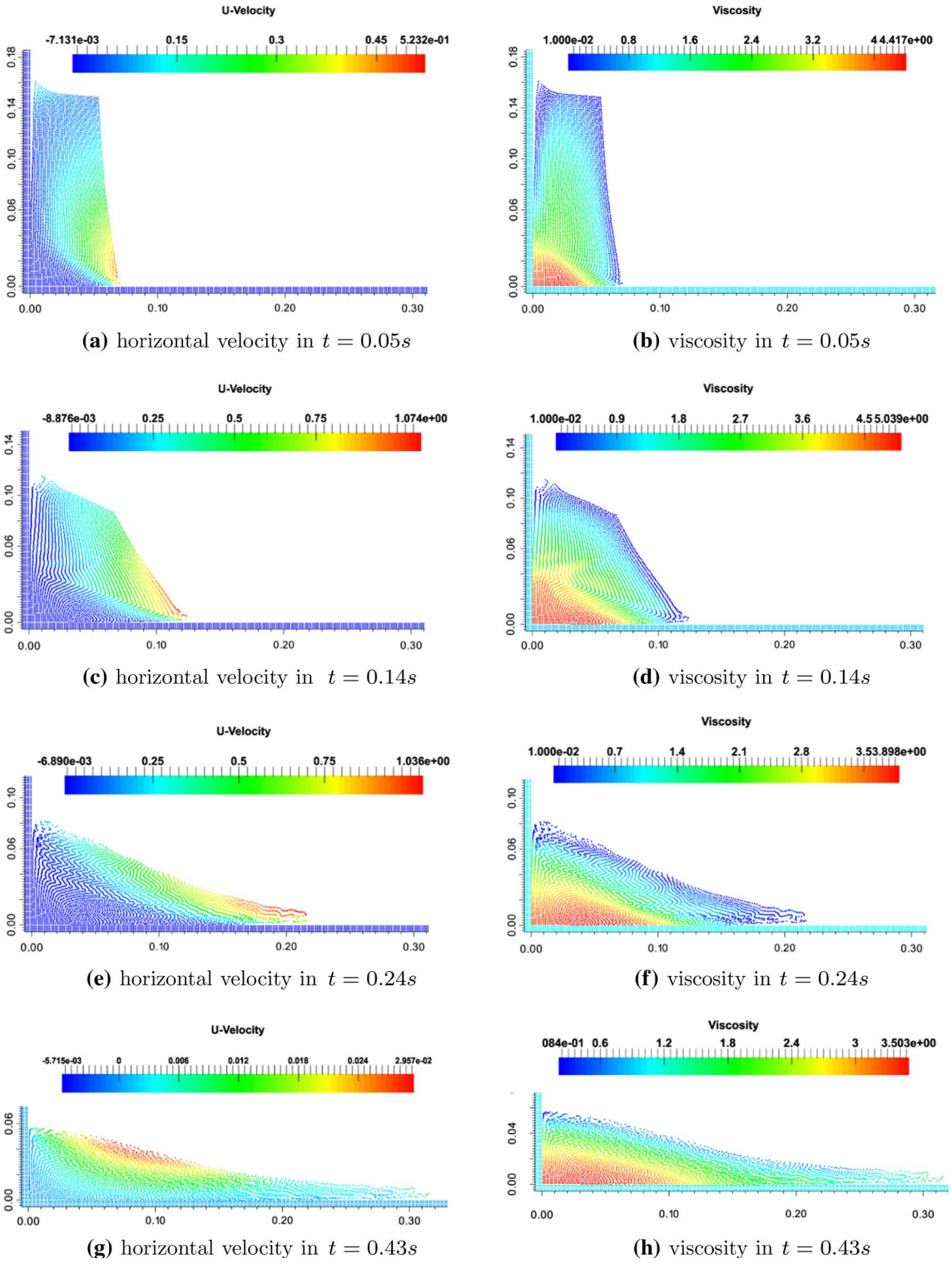

(a) horizontal velocity in $t = 0.05s$ **(b)** viscosity in $t = 0.05s$

(c) horizontal velocity in $t = 0.14s$ **(d)** viscosity in $t = 0.14s$

(e) horizontal velocity in $t = 0.24s$ **(f)** viscosity in $t = 0.24s$

(g) horizontal velocity in $t = 0.43s$ **(h)** viscosity in $t = 0.43s$

Fig. 16 horizontal velocity (ms^{-1}) (left column) and pressure (Pa) (right column), calculated with variable viscosity with the $\mu(I)$ rheology at different times for granular dam-breaking for $a = 3.2$

failure mechanism consists of the avalanche of the outside column edge, leaving the column inside undisturbed; a cone deposit is left for the column. while for high column ratios, the whole granular column collapses completely, resulting in the final deposit looks like a Mexican-hat. In all cases, there was a triangular wedge (or trapezoidal wedge for low

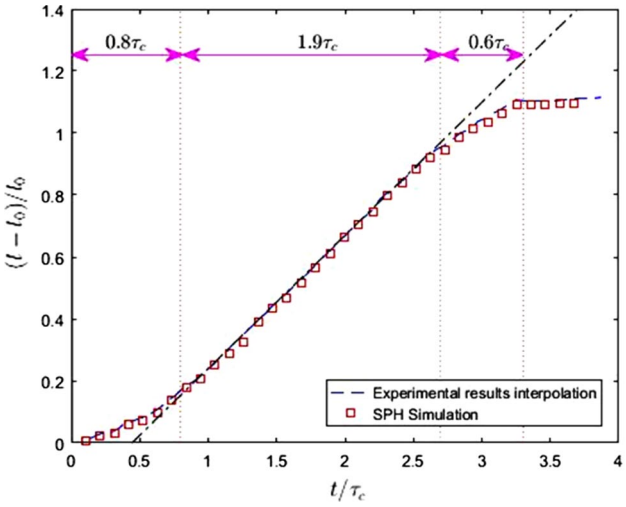

Fig. 17 Wave front time evolutions of glass beads compared with scaling from Lajeunesse et al. [1, 2] for $a = 0.6$

aspect ratio columns) which has the basal width larger than the column one and make an angle with the horizon, within which the grains never move.

Except in the vicinity of the column base where the flow is in resting, the measured velocity profiles are similar to those that are usually observed in static granular surface flows. The velocity varies linearly in the flowing layer while decreasing exponentially in the interface with the static region. The wave front time evolutions show when the flow is fully developed ($t > \tau_c$), the wave front approximately travels in a constant velocity, along the slope line independent of the initial column ratio which presents in Fig. 17.

8 Conclusions

In this paper, with the objective of modeling free-surface flows, a constitutive law describing dense granular materials is implemented within the SPH framework. The dense granular flow is characterized as a pressure-dependent viscoplastic material by this constitutive law, with an apparent viscosity depending on local pressure and the norm of strain rate. Due to the pressure-dependent rheology, The pressure oscillations could be converted into perturbations of flow velocity and free-surface shape. Hence, a modified SPH algorithm proposed to reduce spurious pressure oscillations in the solution. The proposed method proved to be robust and more stable for the problems solved.

The SPH model has been validated by reproducing analytical solution of the uniform flows down an inclined plane and simulating granular spreading on a horizontal bed with excellent accuracy. The simulation results are found to be in good agreement with available experimental observations. In the vicinity of free surfaces, and in particular fluid fronts, where the level of numerical noise remains relatively high, implementation of the modified SPH algorithm and consistency corrections [38, 43] can be effective. Using of eddy viscosity assumption was able to handle higher velocity flow problems that happened at large column ratios. Increasing the value of apparent viscosity in static and stopping regions leads to a reduced time step so a new viscosity regularization method has been proposed to be capable of reproducing yield condition within the reasonable approximation.

Compliance with ethical standards

Conflict of interest The authors declare that they have no conflict of interests.

References

1. Lajeunesse, E., Mangeney-Castelnau, A., Vilotte, J.P.: Spreading of a granular mass on a horizontal plane. Phys. Fluids **16**(7), 2371–2381 (2004)
2. Lajeunesse, E., Monnier, J.B., Homsy, G.M.: Granular slumping on a horizontal surface. Phys. Fluids **17**(10), 103302 (2005)
3. Lube, Gert, Huppert, Herbert E., Sparks, R.Stephen J., Hallworth, Mark A.: Axisymmetric collapses of granular columns. J. Fluid Mech. **508**, 175–199 (2004)
4. Lube, Gert, Huppert, Herbert E, Sparks, R Stephen J, Freundt, Armin: Collapses of two-dimensional granular columns. Phys. Rev. E **72**(4), 041301 (2005)
5. Lube, Gert, Huppert, Herbert E, Sparks, R Stephen J, Freundt, Armin: Static and flowing regions in granular collapses down channels. Phys. Fluids **19**(4), 043301 (2007)
6. Pouliquen, Olivier: Scaling laws in granular flows down rough inclined planes. Phys. Fluids **11**(3), 542–548 (1999)
7. Mangeney, A., Roche, O., Hungr, O., Mangold, N., Faccanoni, G., Lucas, A.: Erosion and mobility in granular collapse over sloping beds. J Geophys Res Earth Surf. **115**(F3), F03040 (2010)
8. Cundall, Peter A, Strack, Otto DL: A discrete numerical model for granular assemblies. Geotechnique **29**(1), 47–65 (1979)
9. Cleary Paul, W., Campbell, Charles S.: Self-lubrication for long runout landslides: examination by computer simulation. J. Geophys. Res. Solid Earth **98**(B12), 21911–21924 (1993)
10. Roberto, Zenit: Computer simulations of the collapse of a granular column. Phys. Fluids **17**(3), 031703 (2005)
11. Staron, L., Hinch, E.J.: The spreading of a granular mass: role of grain properties and initial conditions. Granul. Matter. **9**(3–4), 205 (2007)
12. Lacaze, Laurent, Kerswell, Rich R: Axisymmetric granular collapse: a transient 3D flow test of viscoplasticity. Phys. Rev. Lett. **102**(10), 108305 (2009)
13. Da Cruz, Frédéric, Emam, Sacha, Prochnow, Michaël, Roux, Jean-Noël, Chevoir, François: Rheophysics of dense granular materials: discrete simulation of plane shear flows. Phys. Rev. E **72**(2), 021309 (2005)
14. Jop, Pierre, Forterre, Yoël, Pouliquen, Olivier: A constitutive law for dense granular flows. Nature **441**(7094), 727–730 (2006)
15. Kamrin, Ken, Koval, Georg: Nonlocal constitutive relation for steady granular flow. Phys. Rev. Lett. **108**(17), 178301 (2012)

16. Drucker, Daniel Charles, Prager, William: Soil mechanics and plastic analysis or limit design. Q. Appl. Math. **10**(2), 157–165 (1952)
17. Lagrée, P.-Y., Staron, Lydie, Popinet, Stéphane: The granular column collapse as a continuum: validity of a two-dimensional Navier–Stokes model with a μ(I)-rheology. J. Fluid Mech. **686**, 378–408 (2011)
18. Kamrin, Ken: Nonlinear elasto-plastic model for dense granular flow. Int. J. Plast. **26**(2), 167–188 (2010)
19. Lucy, Leon B.: A numerical approach to the testing of the fission hypothesis. Astron. J. **82**, 1013–1024 (1977)
20. Gingold, Robert A., Monaghan, Joseph J.: Smoothed particle hydrodynamics: theory and application to non-spherical stars. Mon. Not. R. Astron. Soc. **181**(3), 375–389 (1977)
21. Randles, P.W., Libersky, L.D.: Smoothed particle hydrodynamics: some recent improvements and applications. Comput. Methods Appl. Mech. Eng. **139**(1–4), 375–408 (1996)
22. Eghtesad, A., Shafiei, A.R., Mahzoon, M.: Study of dynamic behavior of ceramic-metal FGM under high velocity impact conditions using CSPM method. Appl. Math. Model. **36**(6), 2724–2738 (2012)
23. Shao, Songdong, Gotoh, Hitoshi: Turbulence particle models for tracking free surfaces. J. Hydraul. Res. **43**(3), 276–289 (2005)
24. Monaghan, Joe J.: Simulating free surface flows with SPH. J. Comput. Phys. **110**(2), 399–406 (1994)
25. Shao, Songdong, Lo, Edmond Y.M.: Incompressible SPH method for simulating Newtonian and non-Newtonian flows with a free surface. Adv. Water Resour. **26**(7), 787–800 (2003)
26. Violeau, Damien, Issa, Reza: Numerical modelling of complex turbulent free surface flows with the SPH method: an overview. Int. J. Numer. Methods Fluids **53**(2), 277–304 (2007)
27. Laigle, Dominique, Lachamp, Philippe, Naaim, Mohamed: SPH-based numerical investigation of mudflow and other complex fluid flow interactions with structures. Comput. Geosci. **11**(4), 297–306 (2007)
28. Pasculli, Antonio, Minatti, Lorenzo, Sciarra, Nicola, Paris, Enio: SPH modeling of fast muddy debris flow: numerical and experimental comparison of certain commonly utilized approaches. Ital. J. Geosci. **132**(3), 350–365 (2013)
29. Bui, Ha H, Fukagawa, Ryoichi, Sako, Kazunari, Ohno, Shintaro: Lagrangian meshfree particles method (SPH) for large deformation and failure flows of geomaterial using elastic-plastic soil constitutive model. Int. J. Numer. Anal. Methods Geomech. **32**(12), 1537–1570 (2008)
30. Nguyen, Cuong T, Nguyen, Chi T, Bui, Ha H, Nguyen, Giang D, Fukagawa, Ryoichi: A new SPH-based approach to simulation of granular flows using viscous damping and stress regularisation. Landslides **14**(1), 69–81 (2017)
31. Pouliquen, Olivier, Cassar, Cyril, Jop, Pierre, Forterre, Yoel, Nicolas, Maxime: Flow of dense granular material: towards simple constitutive laws. J. Stat. Mech. Theor. Exp. **2006**(07), P07020 (2006)
32. Xu, Rui: An improved incompressible smoothed particle hydrodynamics method and its application in free-surface simulations. PhD thesis. University of Manchester (2010)
33. Gotoh, Hitoshi, Shibahara, Tomoki, Sakai, Tetsuo: Sub-particle-scale turbulence model for the MPS method - Lagrangian flow model for hydraulic engineering. Adv. Methods Comput. Fluid Dyn. **9**, 339–347 (2001)
34. Dalrymple, R.A., Rogers, B.D.: Numerical modeling of water waves with the SPH method. Coast. Eng. **53**(2), 141–147 (2006)
35. Abdelrazek, Ahmed M, Kimura, Ichiro, Shimizu, Yasuyuki: Simulation of three-dimensional rapid free-surface granular flow past different types of obstructions using the SPH method. J. Glaciol. **62**(232), 335–347 (2016)
36. Gui-Rong, Liu, Liu Moubin, B.: Smoothed particle hydrodynamics: a meshfree particle method. World Scientific, Singapore (2003)
37. Monaghan, Joseph J., Lattanzio, John C.: A refined particle method for astrophysical problems. Astron. Astrophys. **149**, 135–143 (1985)
38. Oger, Guillaume, Doring, Mathieu, Alessandrini, Bertrand, Ferrant, Pierre: An improved SPH method: towards higher order convergence. J. Comput. Phys. **225**(2), 1472–1492 (2007)
39. Monaghan, Joe J.: Smoothed particle hydrodynamics. Rep. Prog. Phys. **68**(8), 1703 (2005)
40. Morris, Joseph P, Fox, Patrick J, Zhu, Yi: Modeling low Reynolds number incompressible flows using SPH. J. Comput. Phys. **136**(1), 214–226 (1997)
41. Xu, Rui, Stansby, Peter, Laurence, Dominique: Accuracy and stability in incompressible SPH (ISPH) based on the projection method and a new approach. J. Comput. Phys. **228**(18), 6703–6725 (2009)
42. Cleary, Paul W., Monaghan, Joseph J.: Conduction modelling using smoothed particle hydrodynamics. J. Comput. Phys. **148**(1), 227–264 (1999)
43. Schwaiger, Hans F.: An implicit corrected SPH formulation for thermal diffusion with linear free surface boundary conditions. Int. J. Numer. Methods Eng. **75**(6), 647–671 (2008)
44. Adami, S., Hu, X.Y., Adams, N.A.: A generalized wall boundary condition for smoothed particle hydrodynamics. J. Comput. Phys. **231**(21), 7057–7075 (2012)
45. Fatehi, R., Manzari, M.T.: A consistent and fast weakly compressible smoothed particle hydrodynamics with a new wall boundary condition. Int. J. Numer. Methods Fluids **68**(7), 905–921 (2012)
46. Goldhirsch, Isaac: Rapid granular flows. Annu. Rev. Fluid Mech. **35**(1), 267–293 (2003)
47. Papanastasiou, Tasos C.: Flows of materials with yield. J. Rheol. **31**(5), 385–404 (1987)
48. Jop, Pierre, Forterre, Yoël, Pouliquen, Olivier: Crucial role of sidewalls in granular surface flows: consequences for the rheology. J. Fluid Mech. **541**, 167–192 (2005)
49. MiDi, G.D.R.: On dense granular flows. Eur. Phys. J. E. **14**(4), 341–365 (2004)
50. Forterre, Yoël, Pouliquen, Olivier: Long-surface-wave instability in dense granular flows. J. Fluid Mech. **486**, 21–50 (2003)